Princeton Plasma Physics Laboratory

PPPL- 4590

PPPL- 4590

Predictions of alpha heating in ITER L-mode and H-mode plasmas

R.V. Budny

January, 2011

Prepared for the U.S. Department of Energy under Contract DE-AC02-09CH11466.

Princeton Plasma Physics Laboratory
Report Disclaimers

Full Legal Disclaimer

Trademark Disclaimer

PPPL Report Availability

Princeton Plasma Physics Laboratory:

http://www.pppl.gov/techreports.cfm

Office of Scientific and Technical Information (OSTI):

http://www.osti.gov/bridge

Related Links:

U.S. Department of Energy

Office of Scientific and Technical Information

Fusion Links

Predictions of alpha heating in ITER L-mode and H-mode plasmas

R. V. Budny*

Princeton Plasma Physics Laboratory, Princeton, NJ 08543

(Dated: March 8, 2011)

Predictions of alpha heating in L-mode and H-mode DT plasmas in ITER are generated using the PTRANSP code. The baseline toroidal field of 5.3 T, plasma current ramped to 15 MA and a flat electron density profile ramped to Greenwald fraction 0.85 are assumed. Various combinations of external heating by negative ion neutral beam injection, ion cyclotron resonance, and electron cyclotron resonance are assumed to start half-way up the density ramp with the full power planned of $P_{\rm ext}$=73 MW. After 50 s the applied power is reduced to 48 MW to increase $Q_{\rm DT}$. The time evolution of plasma temperatures and, for some cases, toroidal rotation are predicted assuming GLF23 and boundary parameters. Conservatively low temperatures ($\simeq$0.6 keV) at the boundary (r/a = 0.85) are assumed. Two alternative options are used to predict the toroidal rotation and flow shearing rate induced by the neutral beam torques in order to get a range of predictions and assess uncertainty. One option assumes the momentum transport coefficient χ_ϕ is half the energy transport coefficient χ_i predicted consistently with the GLF23-predicted temperatures. In this case flow shearing does not have significant effects on the energy transport, and the alpha heating powers for the various heating mixes are predicted to be 8-20 MW (with $P_{\rm ext}$=73 MW). The second option uses GLF23 to also predict toroidal rotation. Significantly higher flow-shearing rates are predicted and the alpha heating power is predicted to be 8-70 MW (with $P_{\rm ext}$=73 MW). External heating mixes with higher beam injection power have higher alpha heating power. If the $L \rightarrow H$ power threshold is twice the ITPA fit then the heating mixes with the highest neutral power (and the most alpha heating) transition to H-mode during the density ramp. Other heating mixes remain in L-mode. Predictions of H-mode temperatures and alpha heating depending sensitively on the assumed pedestal temperatures. A scan in pedestal temperatures is presented using the more pessimistic option assuming $\chi_\phi/\chi_i = 0.5$. Cases with $P_{\rm ext}$=48 MW and fusion gain greater than 10 are predicted to have alpha heating greater than 80 MW.

PACS numbers: 07.05.Tp, 28.52.Av, 28.52.-s, 28.52.Cx, 52.55.Pi

1. Introduction

One of the goals of ITER [1] experiments will be to produce H-mode plasmas with a fusion gain $Q_{\rm DT}$ (the ratio of the DT fusion and the external heating powers $P_{\rm DT}/P_{\rm ext}$) ≥ 10. Enhanced confinement regimes such as in the H-mode appear necessary to achieve this, but the physics basis for the $L \rightarrow H$ transition as well as confinement enhancement remain unclear, and extrapolations of the database scaling might not be reliable for predicting the heating power needed for the transition. Thus having the capability of large amounts of external heating power would increase the chances of success. The planned heating and current drive systems for ITER are: Negative ion Neutral Beam Injection (NNBI), Ion Cyclotron Resonance Frequency (ICRF), and Electron Cyclotron Resonance Frequency (ECRF) with maximum total power of 73 MW. Lower-hybrid current drive (LHCD) is planned as a possible later upgrade.

This paper uses the PTRANSP code [2–4] to generate time-dependent integrated predictions of ITER L-mode and H-mode plasmas. The time dependence is modeled to include long-term trends and to obtain predictions of both the L-mode and H-mode phases. Several expressions for the H-mode power threshold are coded into PTRANSP. The one used here is based on a database fit [5]

$$P_{\rm MW} = 2.15\kappa^{\pm 0.107} n_{\rm e20}^{0.782\pm 0.037} B_{\rm tesla}^{0.772\pm 0.031} a_{\rm m}^{0.975\pm 0.08} R_{\rm m}^{0.999\pm 0.01} 2.0/M_{\rm AMU} \qquad (1)$$

Here κ is the elongation of the boundary. This expression is multiplied by either two or four for use in the L-mode studies. Note with this scaling $P_{L\rightarrow H}$ decreases with decreasing density indicating that it could be beneficial for ITER to start NNBI injection early. However various experiments indicate a tokamak- and configuration-dependent minimum in density [6–9] not given by this scaling. It is unclear where this density minimum would occur in ITER. Injection is started at half the flat top density in this study. Full-power beam injection can not start too early since the beam shine-through could damage the first wall. In PTRANSP a power threshold for the back transition $P_{H\rightarrow L}$ is also modeled and the H-mode phase is terminated when $P = P_{\rm ext} + P_{\alpha}$ decreases below some pre-set factor of $P_{L\rightarrow H}$. The default factor 75% is used here.

The full external power $P_{\rm ext} = 73$ MW is sufficient to achieve the H-mode assuming Eq. 1. With that power only a brief transient L-mode phase is expected. The alpha heating during the Ohmically-heated L-mode at half density is predicted to be relatively small ($\simeq 0.3$ MW).

In this paper the predictions for the L-mode assume pessimistic cases in which the power threshold is higher than the database scaling $\rm P_{Eq1}$ (Eq.1) by a factor of two or four. Even with a factor of two, $P_{\rm ext} = 73$ MW would be

insufficient alone, and additional alpha heating would be necessary to achieve the H-mode. Thus the power from alpha self-heating in the L-mode phase could play a crucial role in achieving the H-mode. In the factor-of-two case only half of the heating mixes considered are predicted to transition to H-mode.

ITER L-mode predictions are in Ref. [4]. Here a wider range of assumptions, both more and less pessimistic are used to explore a range of possibly results in ITER. Predictions of ITER H-mode $P_{\rm DT}$ with a scan in boundary temperatures T_{ped} are in Ref. [2]. Here a wider scan in the equivalent $\beta_{n,ped}$ is studied and results for a wider range of plasma parameters are given.

2. Plasmas Studied

Six mixes of external heating are considered, as summarized in Table I, with heating power waveforms plotted in figure 1. The first five are similar to those considered in Ref. [4]. Each NNBI beam line is specified to deliver up to $P_{\rm NB}$=16.5 MW of 1 MeV D. The baseline design includes two beamlines, but a third beamline is being considered as a contingency for ITER. The case with only ECRF is not being considered for ITER, but has been discussed as an alternative in case the NNBI and ICRF developments do not succeed. Comparisons of the merits of four similar mixes of heating are discussed in [10].

The NUBEAM module [11] in PTRANSP is used to simulate the NNBI heating, torquing, and current-drive, and alpha heating. Below-axis beam NNBI steering is assumed, with the center of the beams displaced 25 cm below the vessel midplane at the "turning point" of minimum major radius, as described in Ref. [2]. The ICRF is assumed to use He^3 minority heating at 52.5 MHz for central heating. The baseline design specifies capability of 20 MW injected power. The TORIC full-wave code [12], coupled into PTRANSP is used to simulate the ICRF heating. TORIC simulations for ITER have been benchmarked with other full-wave solvers [13]. The planned ECRF heating and current drive frequency is 170 GHz, launched in O-mode. The baseline design specifies capability of 20 MW injected power. Three midplane launchers and two upper launchers (for Neoclassical Tearing Mode suppression) are planned. The assumed launcher positions and angles are those in Table 2 of Ref. [4]. The TORAY-GA code [14–16] is used to model the heating and current drive.

Standard assumptions are used for the toroidal magnetic field $B_{\rm tor} = 5.3$ T, plasma current $I_{\rm p}$ ramped to 15 MA, and Greenwald fraction $\bar{n}_e/\bar{n}_{\rm GW}$ (with $\bar{n}_e$ the line-average, and $\bar{n}_{\rm GW} \equiv I_{\rm p}/(\pi a^2) \times 10^{20}/{\rm m}^3$) ramped to 0.85. The assumed ramp-up of the central electron density and the computed ion densities are shown in Fig. 2-a). In PTRANSP the

sum of the thermal deuterium and tritium density profiles is computed from the assumed n_e and the computed fast ion and impurity densities. The separate n_D and n_T profiles are computed using one of a variety of user-controlled mixing models. The model used for this study specifies relative diffusivities and pinches for the D and T. This choice has been used to analyze DT experiments in TFTR and JET, and predicts the DT neutron emission in approximate agreement with measurements using neutron colluminators. The prediction for ITER is that the n_D and n_T are nearly equal. The plasma current and various components are shown in Fig. 2-b).

Previous PTRANSP papers [2–4] use physics-based models to predict profiles of the temperatures T_e and T_i, and in some cases, the toroidal rotation $v_{\rm tor}$. The GLF23 model [17] is used here. An improved model TGLF [18] achieves more accurate predictions of temperatures measured in DIII-D, JET, and TFTR. The code requires parallel processing because it is a longer calculation per call than GLF2, and it has not yet been coupled into a comprehensive self-consistent transport code. GLF23 does achieve approximate agreement predicting temperatures and toroidal rotation. Examples of predictions are in Ref. [19].

There are various options and adjustable parameters for running GLF23. The most extensively tested options use measured toroidal rotation rates to compute flow-shearing rates and use these rates to predict ion and electron temperatures. Alternatively the toroidal rotation can be predicted and used to compute flow-shearing rates which can be used to predict self-consistently ion and electron temperatures. Both options are used here to compute the toroidal rotation to give an indication of effects of uncertainty of the physics. For Option 1 the toroidal rotation is predicted assuming that the ratio of the momentum transport χ_ϕ to the GLF23-predicted ion energy conductivity χ_i is 0.5, which is about midway between values measured in tokamaks with co-plasma-current neutral beam injection. The χ_i profile is calculated in GLF23 consistently with the flow shear taken into account. For Option 2 the toroidal rotation is predicted by GLF23.

In Option 2 the predictions of temperatures and toroidal rotation are consistent. These predictions have been tested Ref. [19], but not as extensively as the predictions of temperatures alone. Predictions for ITER using flow shear from Option 2 suggest the possibility of significant improvement of $Q_{\rm DT}$ in ITER H-mode plasmas [20]. The momentum predictions of GLF23 do not have as rigorous a physics basis Ref. [21] as do the temperature predictions. Nevertheless both options are used here for the L-mode predictions to illustrate ranges of uncertainties in ITER performance predictions. This option gives more optimistic predictions for ITER L-mode plasmas with the heating mixes using NNBI.

The flow shearing rate in GLF23 is a constant times the gradient of the $E \times B$ velocity. the profile of E is computed by force balance of the pressure gradient and the Lorentz force computed using the toroidal and poloidal magnetic fields, the the toroidal and poloidal velocities. The latter is gotten using NCLASS [22]. The value of 1.35 for the constant is usually used in comparing with experiments. Here it is assumed to be unity, to be conservative. The toroidal rotation is computed using GLF23 and the torques predicted for the NNBI. The boundary values for the temperatures and toroidal rotation are taken at the flux surface with x (defined as the square-root of the normalized toroidal flux) at 0.85. The profile of χ_i is assumed to be neoclassical in the core since GLF23 is not valid there.

Sawtooth mixing is predicted to have significant effects on the fast alpha particles. Sawteeth effects are modeled using a Kadomtsev-like mixing with a period assumed to be 10 s. The sawtooth mixing model used here is consistent with evidence of alpha mixing measured in TFTR [23]. Details are given in Section 3.2 of Ref. [2]. The impurities are assumed to be Be, Ar, and He ash. The Be and Ar density profiles are assumed to be 2% and 0.12% of the electron density n_e. Ash transport and recycling are also modeled following Ref. [2]. The ash recycling coefficient is assumed to be 0.7, and the ash diffusivity is assumed to be 1 m^2/s with an inward pinch of 1 m/s. The poloidal field diffusion and Ohmic heating are calculated using neoclassical resistivity predicted by NCLASS, and the calculated T_e and Z_{eff} profiles. Radiation losses and effects of charge-exchange losses due to collisions with recycled neutrals are included. The total radiation loss is predicted to be about 30 MW. The total net charge-exchange loss is predicted to be confined to the edge region beyond x = 0.9 and to be relatively small. The atomic cross sections used are those from the ADAS project [24, 25].

3. Results for the L-mode phase

Evolutions of the predicted central rotation using Option 1 and assuming high $P_{L \to H}$ are shown in Fig. 3-a). These rotation rates are modest compared with rates often measured in tokamaks with neutral beam injection delivering net torque. The temperatures at the boundary for the L-mode are assumed to be pessimistically low, as shown in Fig. 4-a). GLF23-predicted temperature profiles are shown in Fig. 5. The thermal ion and electron heating integrated to the edge region is plotted in Fig. 6-a). The differences of the flows predicted for the different heating mixes is relatively small, indicating that flow shear suppression effects are small.

Plots of P_α(t) are shown in Fig. 7-a). The peak P_α is ~17 MW (for the mix 3NB/IC) and decreases after 50s (at 130 s) when $P_{\rm ext}$ is reduced. The peak $P_{\rm DT}$ is 88 MW for the heating mix 3NB/IC with $P_{\rm ext}$ = 73 MW. The

values of P_α at the end of the high $P_{\rm ext}$ phase are listed in Table II. Plots of $Q_{\rm DT}$(t) are shown in Fig. 8-a). It is below unity for mixes with two or fewer beam lines. $Q_{\rm DT}$ is 1.3 for the heating mix 3NB/IC up to 300 s, and is higher during the sawtooth-induced transients in the late phase when $P_{\rm ext}$ is reduced to 33 MW. After 300 s the relatively large beam-driven current conspires to keep the q profile sufficiently nonmonotic to prevent two of each three specified sawtooth trigger times from mixing. This leads to large sawtooth mixing over a very large radius. There is considerable uncertainty of what to expect if these conditions occur in ITER.

With Option 2 much higher toroidal rotation rates and fusion yields are predicted. First consider the case where $P_{L\rightarrow H}$ is higher than $P_{\rm ext}$ for all the heating mixes. Central rotation rates are shown in Fig. 3-b). The boundary temperatures are the same as those used for Option 1 and shown in Fig. 4-a). The peak temperatures are shown in Fig. 9. The ion temperatures are relatively high for the heating mixes with high NNBI power (and relatively large toroidal rotation rates). The peak values occur as the density is ramping up. Similar phenomena are observed in the supershot regime in TFTR and the hot ion H-mode in JET. This results from the stiffness of GLF23 and the flow shear suppression. Large central temperatures could be expected in ITER as a consequence of the large minor radius and stiff temperature profiles. If there is a lower bound for the temperature gradients then even even with low boundary temperatures, the central ion temperature is predicted to be high. Profiles at one time near peak central temperatures are shown in Fig. 10.

The thermal ion and electron heating densities volume-integrated to the boundary region are plotted in Fig. 6-b). The external heating is relatively constant in the initial phase, but the alpha heating increases as the density and temperature increase. Plots of P_α(t) are shown in Fig. 7-b). The alpha heating reaches 70 MW in the heating mix with three beam lines. The values of P_α at the end of the high $P_{\rm ext}$ phase are listed in Table II. The alpha heating decrease in the next phase with reduced external power. Profiles of the alpha electron and thermal ion heating for two of the heating mixes are compared in Fig. 11 with the profiles of the DT power divided by five. The factor of five is the ratio of the energies carried by alphas and neutrons to when the He^5 resonance decays. The $P_{\rm DT}$ and P_α profiles are predicted to have nearly identical shapes except during transients. $P_{\rm DT}$ is the instantaneous fusion power whereas P_α depends on the slowing down of the alphas. No anomalous diffusion for the fast alpha particles is assumed, and the classical slowing-down and pitch angle scattering have relatively small effects on their profiles. Results for the heating profiles for the six heating mixes near the peak temperatures are shown in Fig. 12. The alpha heating profiles are included in the total electron and thermal ion heating profiles. The cases are ordered approximately in

diminishing alpha heating and $P_{\rm DT}$, indicated by Table II. The higher values result from higher $P_{\rm DT}$.

Next consider Option 2 with $P_{L\to H}$ scaled up a factor of two instead of four. Three of the heating mixes transition to H-mode and three do not. The thermal ion and electron heating densities volume-integrated to the boundary region are plotted in Fig. 6-c), and the total alpha heating in Fig. 7-c). When the plasma transitions to H-mode the PEDESTAL module [26] in PTRANSP is used to predict the pedestal width and the pressure at the top of the pedestal. Since the electron density is prescribed, the pressure determines the pedestal temperatures. These values can be scaled, and for these runs the flat top values of both the ion and electron temperatures are 4.6 keV.

The times of the $L \to H$ are listed in Table II. The total alpha heating is also given in Table II. Their values increase as the transition time increases, mainly due to the increase in density. Note that the alpha heating remains high after the $H \to L$ transition, $P_\alpha \simeq 80$ MW. This appears to be the maximum achievable in L-mode, so the maximum heating power for achieving the H-mode at flat top density is 73 + 80 MW. The corresponding results for the total fusion power are shown in Fig. 7-c).

The values of $Q_{\rm DT}$ are shown in Fig. 8-b). The mix 3NB/IC achieves $Q_{\rm DT}$ of 7.0 with $P_{\rm ext} = 73$ MW, and 3.0 when $P_{\rm ext}$ is lowered to 47 MW. The back transition is assumed to occur if the heat flow decreases below 75 % of $P_{L\to H}$. The times for the three mixes that obtain H-mode are listed in Table II. Note that the mixes with more NNBI power achieve the H-mode earlier and have higher alpha heating. This shows a clear advantage of more beam power. In contrast this advantage is predicted to be more modest during the flat top phases and far from critical values Ref. [2].

Ranges of $< \beta_n >$, stored energy, and confinement parameters are given in Table III. Here $< \beta_n >$ is the volume-average of β_n defined by $\beta_{tor} aB/I$ where B is the vacuum magnetic field averaged over the plasma volume, and β_{tor} is defined as $P/(8\pi B^2)$ with P the local total pressure. The values for the normalized energy confinement times are compared with values extrapolated from the H98y2 scaling relation [27] derived from a multi-tokamak database of ELMing H-mode plasmas maintained by the ITPA confinement working group. The values of H98y2 measured in L-mode plasmas tend to be around 0.5. The values computed from the PTRANSP runs range from 0.24 to 0.33 with Option 2, and 0.24 to 0.40 with Option 1. These are lower than 0.5×H98y2 as a consequence of the pessimistically assumed low boundary temperatures as shown in Fig. 4-a).

4. Results for the H-mode phase

For the H-mode predictions GLF23 is used for the plasma temperatures, but not for the toroidal rotation. The momentum transport is assumed to be related to the ion energy conductivity by $\chi_\phi/\chi_i = 0.5$, as in Option 1 used for the L-mode study. With the PTRANSP-NUBEAM predictions of the NNBI torques, the toroidal rotation is predicted to be relatively low ($\simeq$ 6 kRad/s) and the flow-shearing rate is predicted to have little effect on the GLF23-predicted temperatures.

The nominal database scaling Eq. 1 for the $L \rightarrow H$ power threshold is assumed. Consequently the transition occurs immediately after the external heating is applied, precluding prediction of alpha heating in L-mode plasmas except during the Ohmic phase.

After the transition to H-mode the pedestal temperatures is predicted by the PEDESTAL module in PTRANSP. Their values are used as boundary values for the GLF23 predictions. The resulting core temperatures depend sensitively on them. Since there is uncertainty about their values, scans were performed for the 2NB/IC/EC heating mix by scaling the pedestal values and predicting the temperatures and alpha heating powers.

The $P_{\alpha-e}$ profiles for the scans are shown in Fig. 13. The $P_{\alpha-e}$ + $P_{\alpha-i}$ time evolutions for the scans are shown in Fig. 14. The $Q_{\rm DT}$ time evolutions for the scans are shown in Fig. 15-a). The scaling of $Q_{\rm DT}$ with $P_{\rm ext}$ shown in Fig. 15-b) is approximately $(P_{\rm ext})^{-1.0}$, close the result $(P_{\rm ext})^{-0.8}$ in Ref. [18] using TGLF with the heating profile shapes held fixed and only $P_{\rm ext}$ is varied. The results here are predicted with the heating profiles calculates self-consistently for each $P_{\rm ext}$. The scaling $Q_{\rm DT} \propto (P_{\rm ext})^{-1.0}$ implies $P_{\rm DT}$ independent of $P_{\rm ext}$ so P_α dominates. This simple scaling of $Q_{\rm DT}$ with $P_{\rm ext}$ is not seen with predictions for ITER H-mode plasmas assumed to have peaked density profiles. For these very slow relaxations of profiles lead to slow increases in the central temperatures and thus $P_{\rm DT}$ so no stationary phases are seen even with constant $P_{\rm ext}$.

The $Q_{\rm DT}$ values during the high $P_{\rm ext}$ phase (73 MW in the interval 80-130 s) are plotted versus the local normalized $\beta_{n,ped}$ in Fig. 16-a). The parameter $\beta_{n,ped}$ is defined as the local β_n at the top of the pedestal, and is proportional to $T_{\rm ped}$ since the n_e profile is fixed. Note that $Q_{\rm DT}$ remains below 10 even with pedestal temperatures of 8.8 keV, which appears too high for practical use in ITER due to large transient loss of power from ELMs. The $Q_{\rm DT}$ when $P_{\rm ext}$ is lowered to 47 MW is shown in Fig. 16-b).

Scaling of $Q_{\rm DT}$ with $(T_{\rm ped})^2$ and equivalently with $(\beta_{n,ped})^2$ was found using TGLF when the heating profiles are

held fixed and only $\beta_{n,ped}$ and T_{ped} are varied [18]. The results here, with the heating profiles being calculates self-consistently at each $\beta_{n,ped}$ give a scaling closer to unity. Predictions for the central temperatures, the volume-averaged $< \beta_n >$, and other variables are shown in Fig. 16. Note that in Fig. 16-b) $\beta_{n,ped}$ rises to values that might indicate instability as the pedestal temperature and $Q_{\rm DT}$ increase. Modeling of the peeling-ballooning stability of the edge [28] indicates that the value $\beta_{n,ped}$ will be limited to $\simeq$ 0.6-0.8.

5. Summary

ITER L-mode plasma performance is studied assuming that the power threshold for the $L \rightarrow H$ transition is higher than the maximum heating power anticipated (73 MW). The GLF23 model is used to predict temperatures. Two alternative options are used to compute the flow-shearing rate for GLF23 to give a range of possibly results in ITER. Option 1 uses the conservative assumption that $\chi_\phi/\chi_i = 0.5$. Option 2 uses GLF23 to predict the toroidal rotation, which predicts higher alpha heating in cases with neutral beam injection. This option predicts considerable higher toroidal rotation rates and, as a result of the flow shearing suppression of transport in GLF23, higher $P_{\rm DT}$. Examples are given of conditions with $L \rightarrow H$ transitions when $P_{\rm ext} + P_\alpha$ exceeds the threshold. Values of P_α = 8-70 MW are predicted.

These results suggest that having as much NNBI power available as possible is a good strategy for ITER. The predictions indicate that higher temperatures and $P_{\rm DT}$ would be expected. If the $L \rightarrow H$ power threshold is high and if the flow-shearing rate is high, as expected with the optimistic option, then more NNBI power could be crucial for the H-mode.

Predictions for the H-mode alpha heating use the conservative option 1. The alpha heating as well as the total fusion power and $Q_{\rm DT}$ are predicted to depend sensitively on the pedestal temperature. The $P_{\rm DT}$ increases approximately linearly with the pedestal temperature. For pedestal pressures compatible with peeling-ballooning simulations, P_α up to 80 MW are predicted.

Improvements in theory and modeling that would strengthen the validity of the predictions are: 1) better models are needed for predicting plasma temperatures, rotation, and density. Density profiles are coupled with performance, so predictions of the transport, including pinches and non-diagonal terms such as thermo-electric diffusivities of the various plasma species are needed. Intrinsic rotation and neoclassical viscosity might be important in ITER. Having the TGLF model coupled to a time-dependent integrated predictive model would be an important improvement over

the GLF23 model used here. 2) better models of anomalous fast-ion transport are needed. These should include effects of MHD, NTM, and TAE modes. 3) improved predictions of the heating, torquing, and current-drive are needed for source terms in the transport calculations.

Acknowledgements

The author wishes to thank P. Thomas, F. Wagner, and S. Zweben for motivating this work. The contributions of the PTRANSP development teams at PPPL, Lehigh, GA, and LNL are greatly appreciated. This research is supported by the U.S. Department of Energy under contract number DE-AC02-09CH11466.

* Electronic address: budny@princeton.edu

[1] R. Aymar, V. Chuyanov, M. Huguet, Y. Shimomura, the ITER JOINT CENTRAL TEAM, and HOME TEAMS, Nucl. Fusion **41** 1301 (2001).

[2] R. V. Budny, R. Andre, G. Bateman, F. Halpern, C. Kessel, A. Kritz, and D. McCune, Nucl. Fusion **48**, 075005 (2008).

[3] F. D. Halpern, A. H. Kritz, G. Bateman, A. Y. Pankin and R. V. Budny, and D. C. McCune, Phys. Plasmas **15** 062505 (2008).

[4] R. V. Budny, Nucl. Fusion **49**, 085008 (2009).

[5] Martin Y.R. and ITPA CMDB H-mode Threshold Database Working Group, J. of Physics Conference Series **123** (2008) 012033.

[6] Andrew, Y., *et al.*, Nucl. Fusion **48** (2006) 479.

[7] Hubbard, A., *et al.*, Plasma Phys. Control. Fusion **40** (1998) 689.

[8] Ryter, F., *et al.*, Nucl. Fusion **49**, 062003 (2009).

[9] Gohil, P., Evans, T. E., Fenstermacker, M. E., *et al.*, Proceedings of the IAEA Conference, Daejeon, 2010, and submitted to Nuclear Fusion.

[10] Wagner F., Becoulet A., Budny R., Erckmann V., Farina D., *et al.*, Plasma Phys. Controlled Fusion **52** (2010) 12044.

[11] A. Pankin, G. Bateman, R. Budny, A. Kritz, D. McCune, A. Polevoi, and I. Voitsekhovitch, Comput. Phys. Commun. **43** 61 (1981).

[12] Brambilla M., Plasma Phys. Controlled Fusion **44** (2002) 2423.

[13] Budny, R.V., Berry, L, Bilato, R., Bonoli, P., Brambilla, M., Dumont, R.J., A. Fukuyama, *et al.,* Proceedings of the IAEA Conference, Daejeon, 2010.

[14] D. B. Batchelor, R. C. Goldfinger, Nucl. Fusion **20** 403 (1980).

[15] A. H. Kritz, H. Hsuan, R. C. Goldfinger, and D. B. Batchelor, 1982 Conf. Proc. 3rd Int. Symp. on Heating in Toroidal Plasmas ECE (Brussels, Belgium) **2** 707 (1982).

[16] R. Prater, D. Farina, Y. Gribov, R. W. Harvey, A. K. Ram, Y.-R. Lin-Liu, E. Poli, A. P. Smirnov, F. Volpe, E. Westerhof, A. Zvonkov, and the ITPA Steady State Operation Topical Group, Nucl. Fusion **48** 035006 (2008).

[17] R. E. Waltz, G. M. Staebler, W. Dorland, G.W. Hammett, M. Kotschenreuther, and J.A Koning, Phys. Plasmas **4** 2482 (1997).

[18] Kinsey, J., Waltz, R., Staebler, G., Proceedings of the IAEA Conference, Daejeon, 2010, and submitted to Nuclear Fusion.

[19] Kinsey, J.E., Staebler, G.M., Waltz, R.E., Phys. of Plasmas, **9** (2002) 1676.

[20] Staebler, G., St. John, H. E., Nuclear Fusion **46** L6 (2006).

[21] Staebler, G., submitted to Physics of Plasmas.

[22] W. A. Houlberg, K. C. Shang, S. P. Hirshman, and M. C. Zarnstorff, Physics of Plasmas **4** (1997) 3230.

[23] B.C. Stratton, R.J. Fonck, G.R. Stratton, R.V. Budny, Z. Chang, F. Wising and A. Ödblom, Nuclear Fusion **36** (1996) 1586.

[24] Anderson H., *et al.*, Plasma Physics and Controlled Fusion **42** (2000) 781.

[25] Summers H. P., "The ADAS User Manual v2.6", http://www.adas.ac.uk/manual.php

[26] Onjun T., Bateman G., Kritz A.H., and Hammett G., Plasma Phys. Controlled Fusion **45** (2003) 1939.

[27] ITER Physics Basis Editors, *et al.,* Nuclear Fusion **39** (1997 2137

[28] Snyder P.B., Wilson H.R., Osborne T.H., and Leonard A.W., Plasma Phys. Controlled. Fusion **46** (2004) A131.

Heating mix	80-130 s	130-300 s	300-400 s	400-500 s
3NB/IC	50-23-0	33-13-0	33-0-0	0-0-4
2NB/EC	33-0-40	17-0-30	17-0-17	0-0-4
2NB/IC/EC	33-20-20	17-10-20	17-0-17	0-0-4
1NB/IC/EC	17-20-37	0-10-37	0-0-33	0-0-4
IC/EC	0-20-53	0-10-36	0-0-33	0-0-4
EC	0-0-73	0-0-46	0-0-33	0-0-4

TABLE I: *The six heating power mixes considered. Values for the NNBI-ICRF-ECRF heating in MW are listed for four time periods.*

Heating mix	Option 1	Option 2	Option 2	Option 2
$P_{L\to H}/P_{Eq1}$	4	4	2	2
	P_α [MW]	P_α [MW]	H-mode span [s]	P_α [MW]
3NB/IC	17.0	70	87.5 - 400.0	32
2NB/EC	13.3	62	108.2 - 400.0	41
2NB/IC/EC	16.6	34	110.1 - 311.0	41
1NB/IC/EC	14.2	28	none	-
IC/EC	12.5	13	none	-
EC	8.4	8	none	-

TABLE II: *Values for P_α [MW] computed at 130 s using Options 1 and 2 with $P_{L\to H}$ scaled by up a factor of four or two. The H-mode is not predicted for these predictions. It is predicted for Option 2 with $P_{L\to H}/P_{Eq1} = 2$ for three of the heating mixes. The time span of the H-mode phase is given, and the values of P_α at the $L \to H$ time are given.*

Heating mix	Option 1	Option 1	Option 2	Option 2
$P_{\rm ext}$ [MW]	73	48	73	48
$< \beta_n >$	0.60 - 0.72	0.55 - 0.68	0.60 - 1.40	0.50 - 0.90
W_{tot} [MJ]	125 - 138	105 - 138	125 - 300	105 - 180
τ_E [s]	1.4	1.8	1.4 - 1.6	1.8 - 2.1
H98y2-prediction	0.24 - 0.33	0.23 - 0.32	0.24 - 0.53	0.23 - 0.40
H98y2-database	0.40 - 0.42	0.38 - 0.41	0.38 - 0.66	0.40 - 0.53

TABLE III: *Ranges of values from the six heating mix predictions for the total stored energy and confinement parameters computed for both options at two values for* $P_{\rm ext}$*: 73 MW near 130s, and 48 MW near 180s. The H-factor H98y2 values are computed from the PTRANSP prediction and from the ITPA database scaling.*

T_{ped}	$T_e(0)$	$T_i(0)$	$Q_{\rm DT}$	P_α
keV	keV	keV		MW
8.8	38.0	42.0	9.5	122
6.0	30.0	29.9	5.5	78
4.8	26.5	23.8	4.2	58
1.7	16.5	15.0	1.5	22
0.7	15.5	13.9	0.7	20

TABLE IV: *Results for the H-mode scan in the early phase with* $P_{\rm ext} = 73$ *MW.* $Q_{\rm DT}$ *is less than 10 since* $P_{\rm ext}$ *is large.*

T_{ped}	$T_e(0)$	$T_i(0)$	$Q_{\rm DT}$	P_α
keV	keV	keV		MW
7.5	34.0	35.5	17.5	113
5.1	26.0	25.0	11.0	77
4.0	22.0	20.3	7.8	57
1.2	13.3	11.8	2.0	18

TABLE V: *Results for the H-mode scan in the flat top phase with* $P_{\rm ext} = 47$ *MW.*

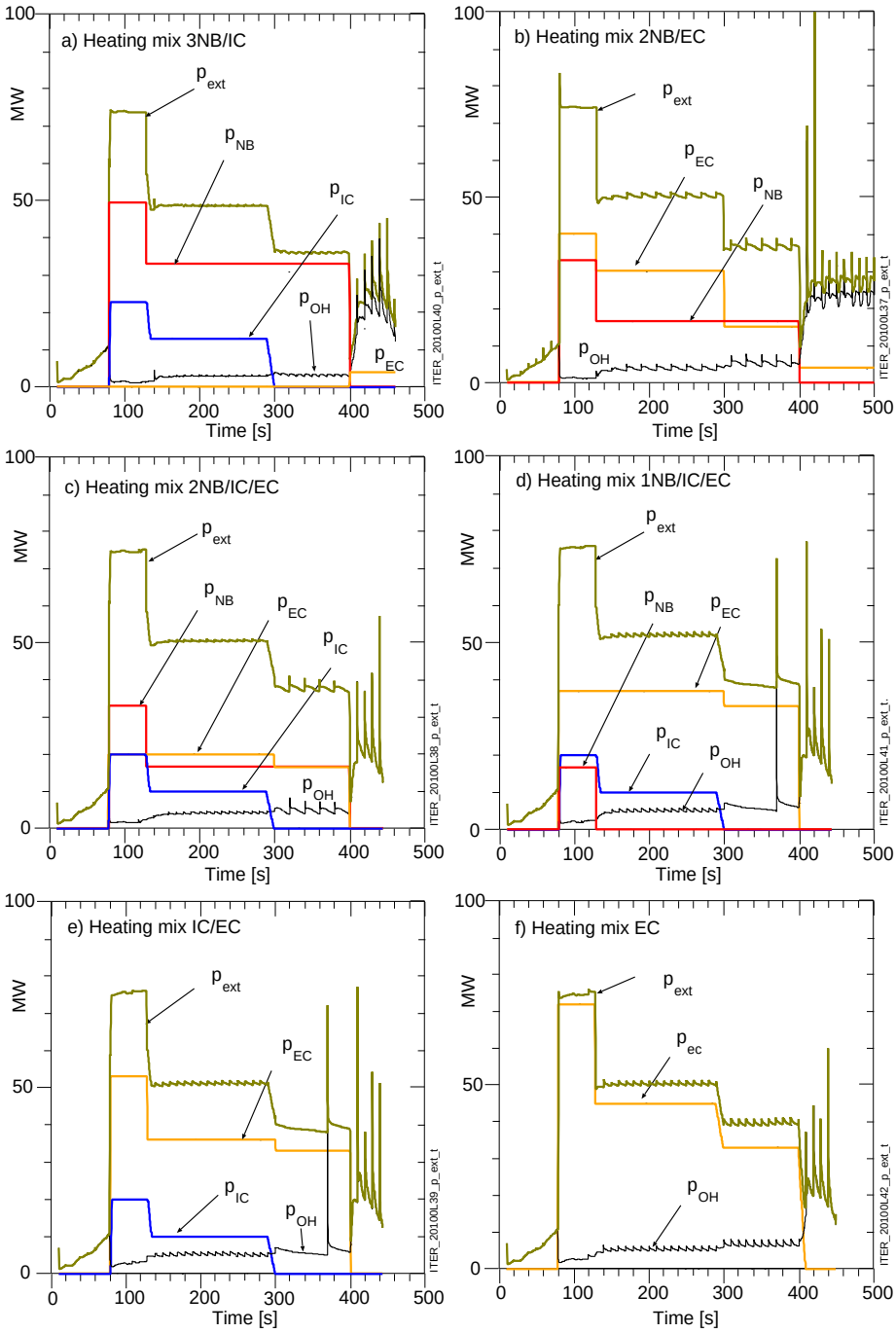

FIG. 1: (Color) Powers for the heating mixes.

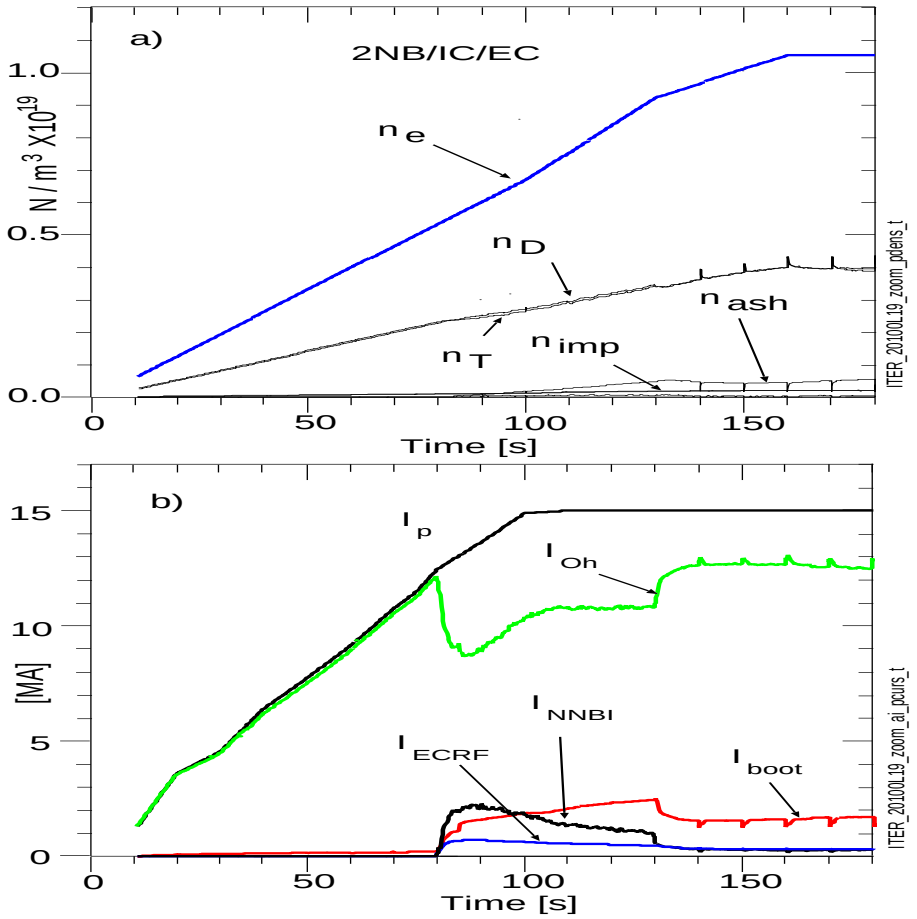

FIG. 2: (Color) a) Assumed central electron density ramped up to $f_{Greenwald} = 0.85$, and computed central ion densities; b) Current ramped up to 15 MA.

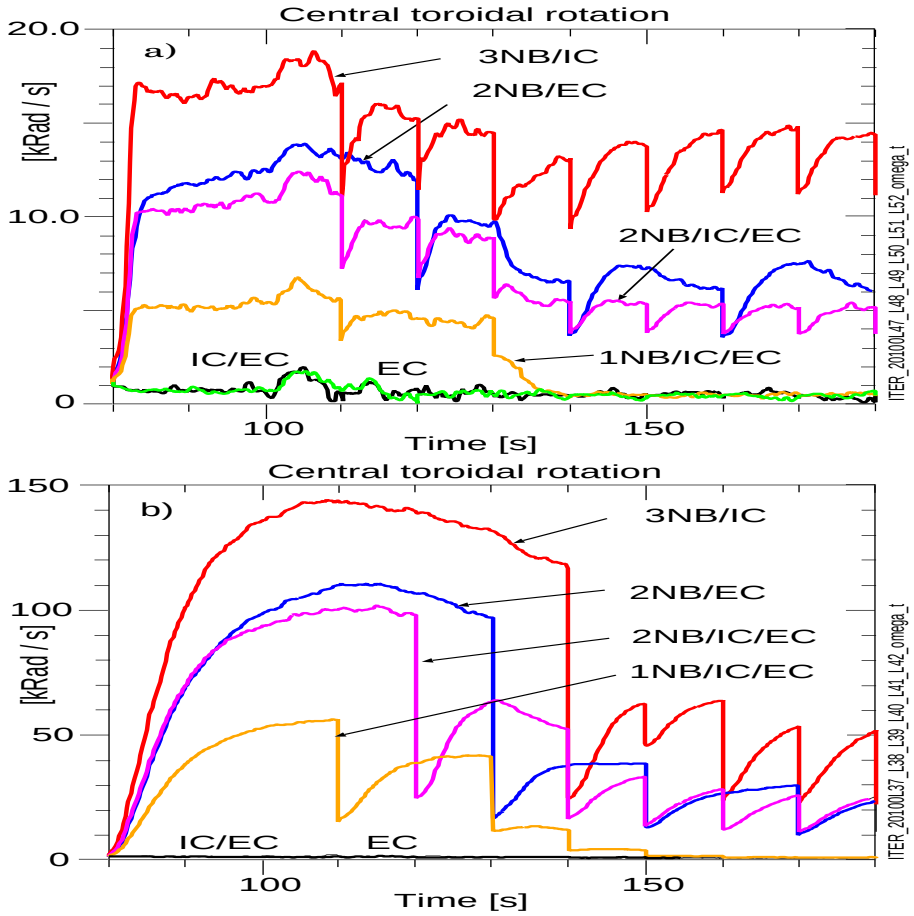

FIG. 3: (Color) Central toroidal rotation for different heating mixes predicted using a) Option 1 ($\chi_\phi = 0.5\chi_i$); b) Option 2 (GLF23 rotation) and $4 \times P_{L\to H}$. The peak rotation is much higher using Option 2, but is comparable to rates measured in some L-mode beam-heated plasmas.

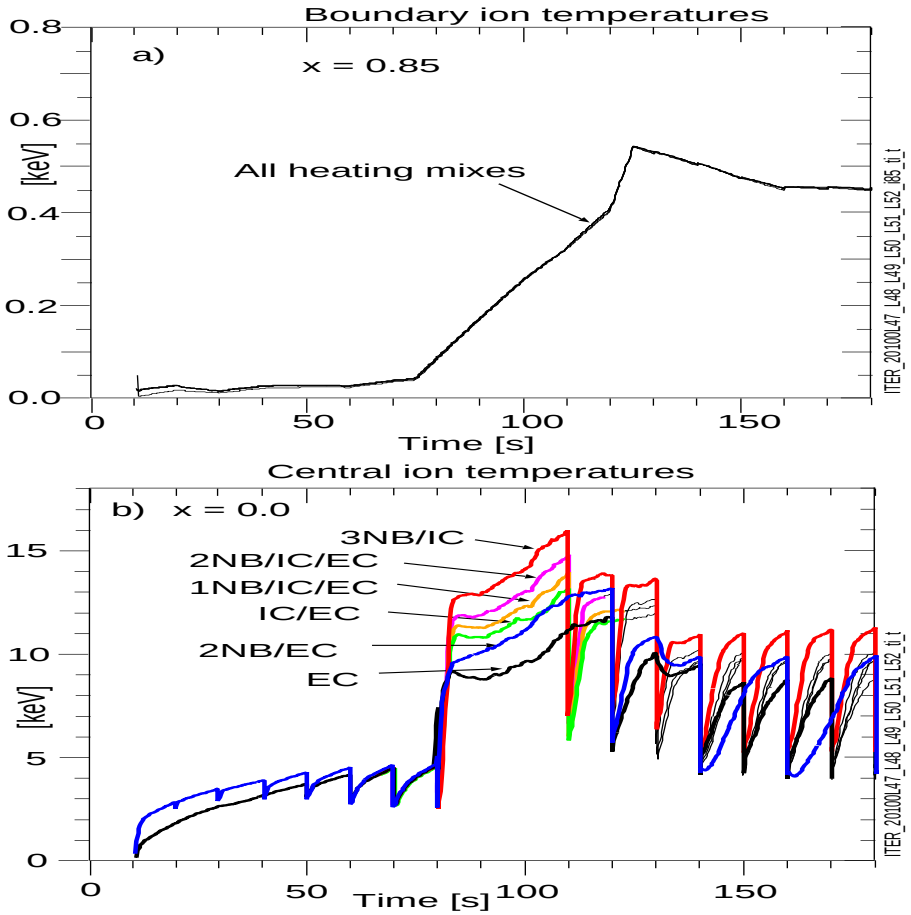

FIG. 4: (Color) Ion temperatures a) assumed at the boundary, and b) computed at the magnetic axis for different heating mixes using Option 1 and high $P_{L\to H}$.

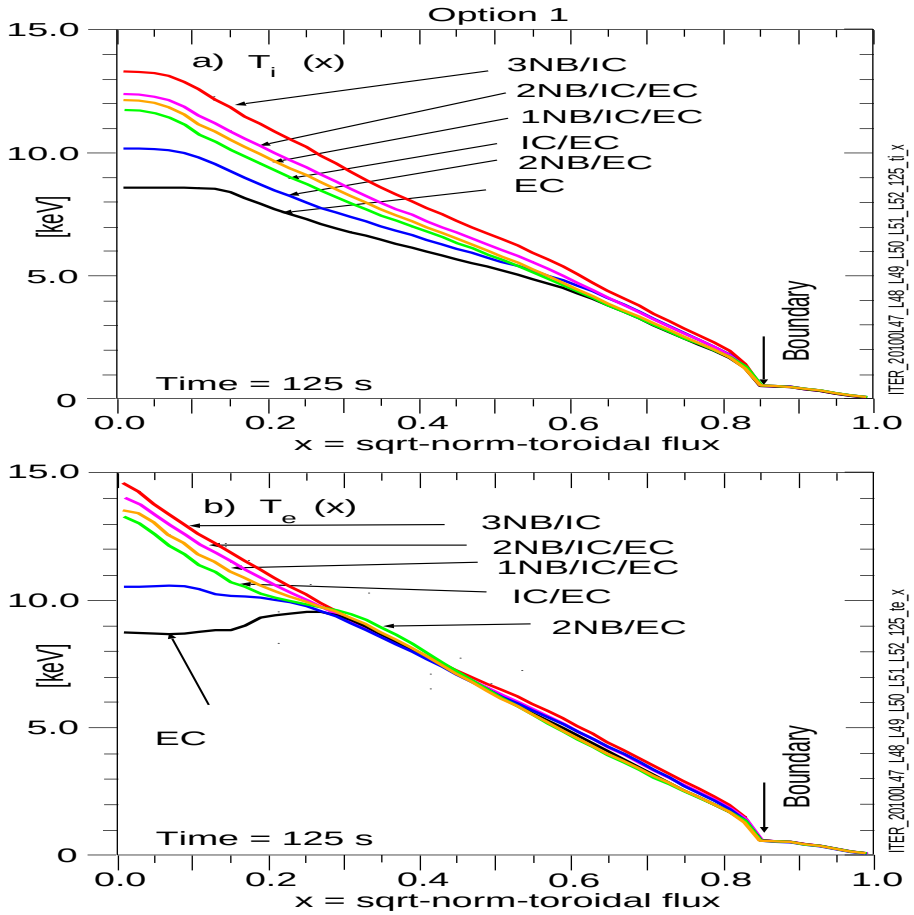

FIG. 5: (Color) a) Ion, and b) electron temperature profiles predicted using Option 1 near the time when they are largest.

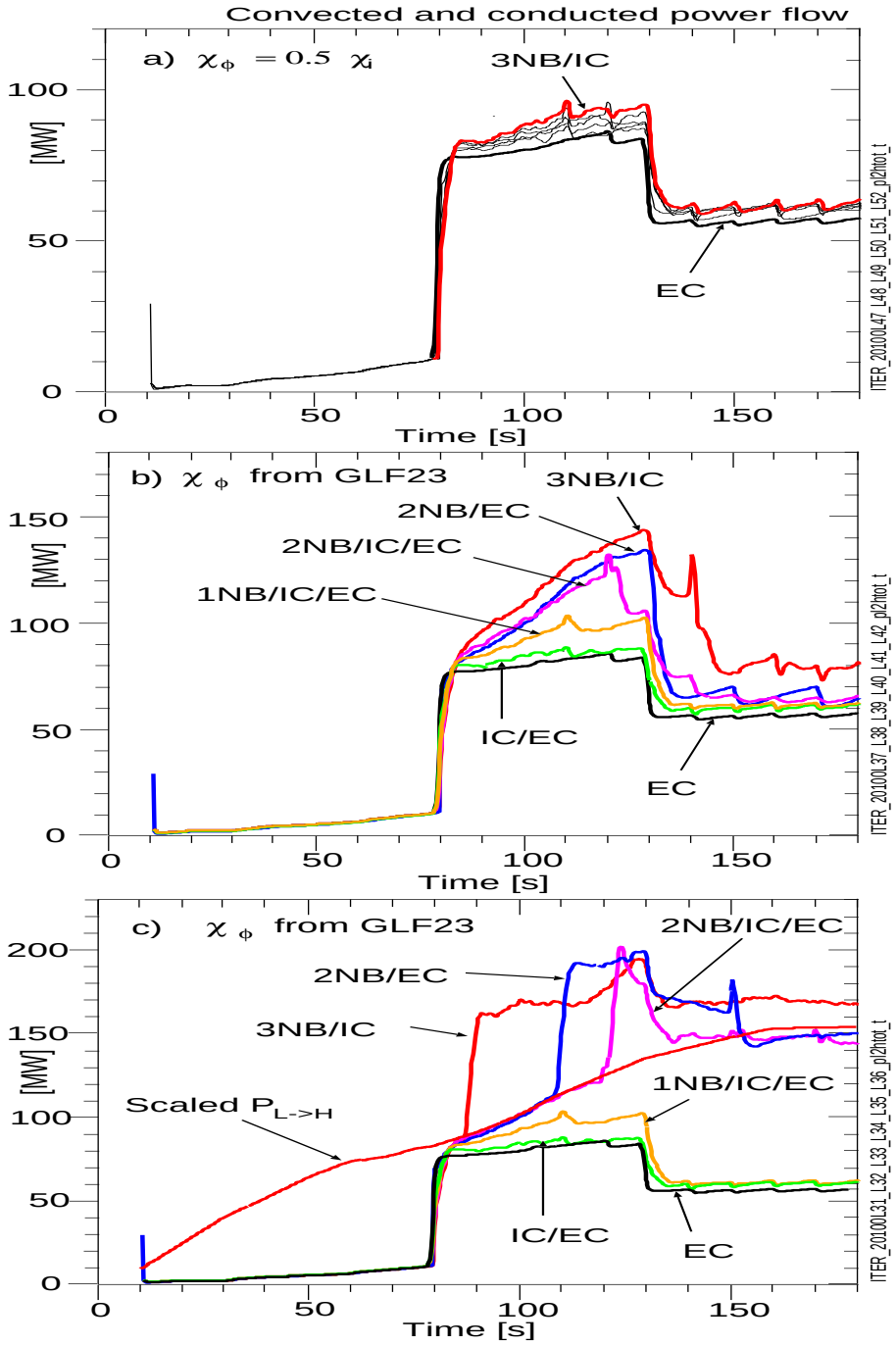

FIG. 6: (Color) Energy flow near the boundary for the six heating mixes; a) Option 1 with the $L \rightarrow H$ power threshold is assumed to be scaled up by a factor of 4 to prevent the H-mode; b) Option 2 with the $L \rightarrow H$ power threshold is assumed to be scaled up by a factor of 4 to prevent the H-mode; c) Option 2 with the $L \rightarrow H$ power threshold is assumed to be scaled up by a factor of 2 which allows three heating mix cases to achieve H-mode during the density ramp; During the H-mode phase, the pedestal temperature is assumed to increase to a flat top value of 4.4 keV, causing the central temperatures and alpha heating to increase.

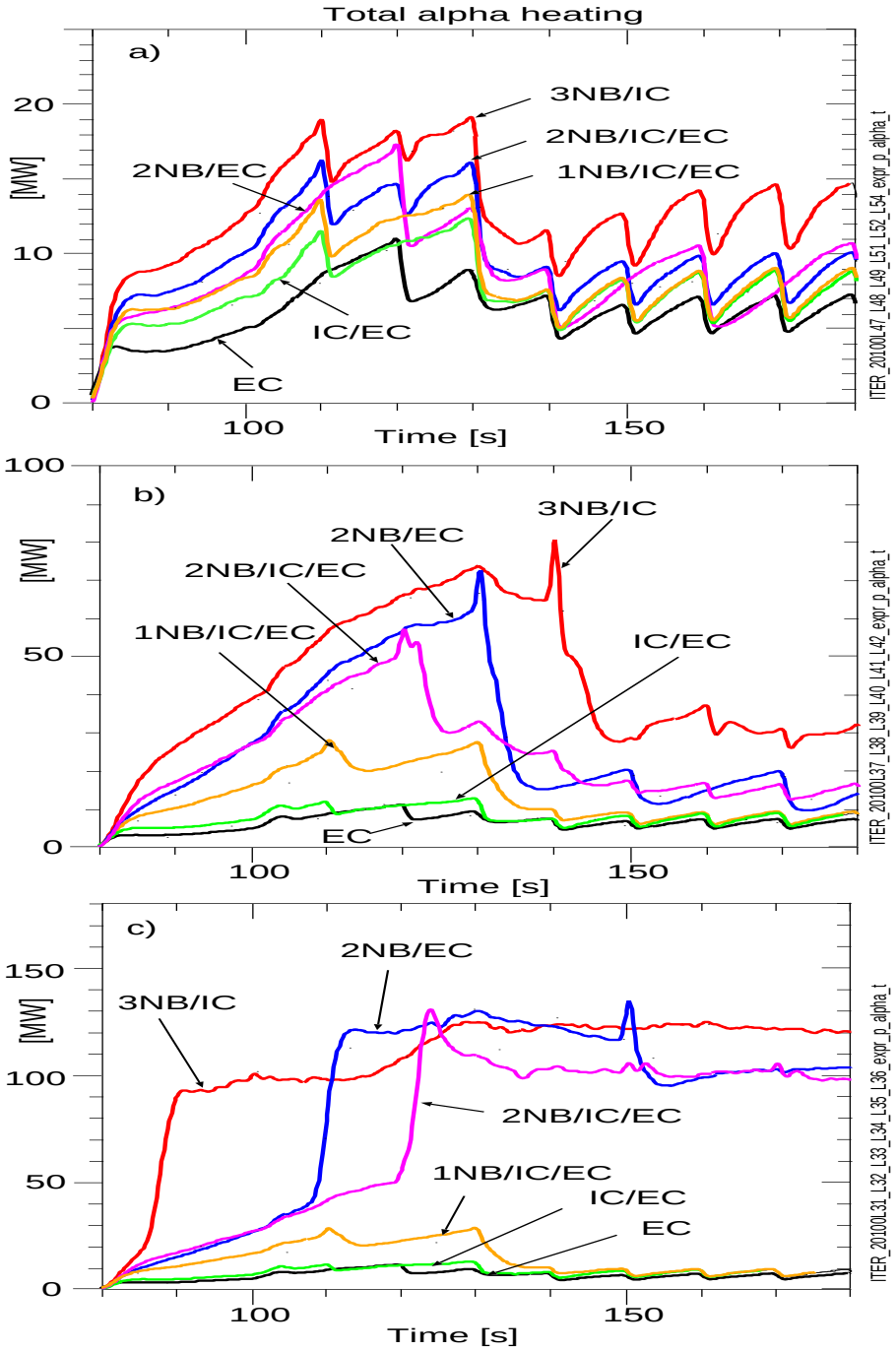

FIG. 7: (Color) Total alpha power to thermal electrons and ions. a) Option 1 with the $L \rightarrow H$ power threshold scaled up by a factor of 4 to prevent the H-mode. b) Option 2 with the $L \rightarrow H$ power threshold scaled up by a factor of 4; c) Option 2 with the $L \rightarrow H$ power threshold scaled up by a factor of 2. The abrupt increases in the alpha heating in c) occur at the times of $L \rightarrow H$. The total alpha heating power is close to the DT fusion power divided by five except for a dwell in time of approximately two sec due to the slowing down of the alpha particles.

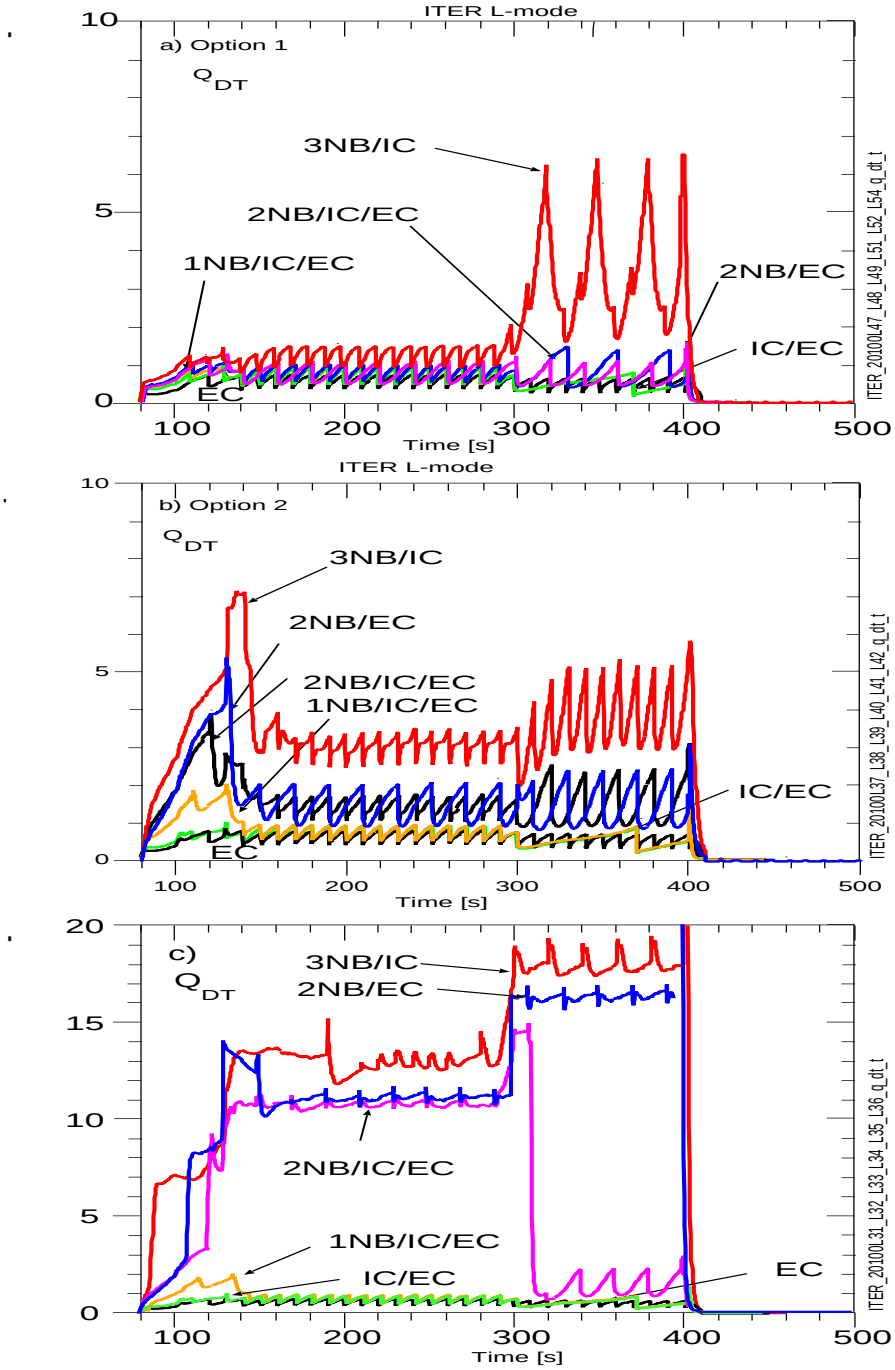

FIG. 8: (Color) Predictions of $Q_{\rm DT}$ using a) Option 1; b) Option 2 with $P_{L\to H}/P_{Eq1} = 4$; c) Option 2 with $P_{L\to H}/P_{Eq1} = 2$. Oscillations in $Q_{\rm DT}$ are caused by sawteeth predicted by Kadomtsev-like mixing at assumed breaks with a 10 sec period. Mixing occurs only if q has just one q = unity surface. The current drive from the NNBI is predicted to have noticeable effects on the q profile. The total beam current from 300 to 400 s is around 350 kA for the 3NB/IC mix, more than twice that of the 2NB/EC and 2NB/IC/EC mixes. The predicted q profiles have large radii for q = unity, especially for the 3NB/IC mix. The large inversion radii (up to x $\simeq$ 0.7) cause large oscillations of the central ion temperature and larger regions of high DT fusion reaction rates.

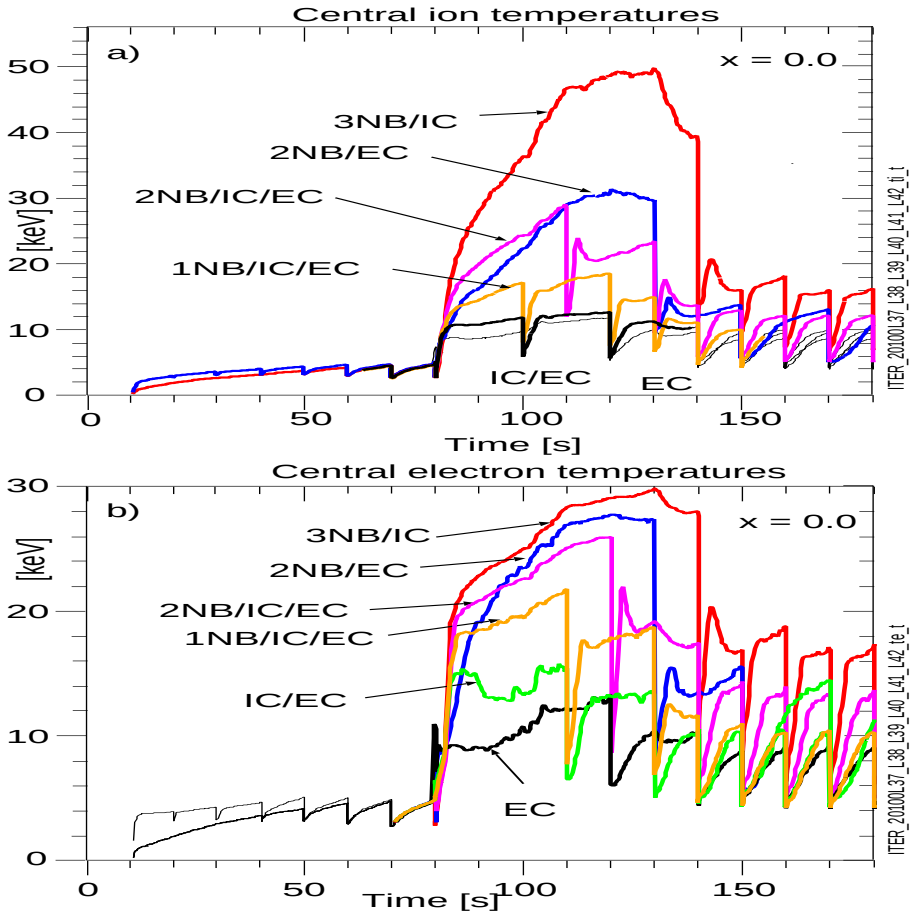

FIG. 9: (Color) Predictions using Option 2 of a) Central ion and b) electron temperatures.

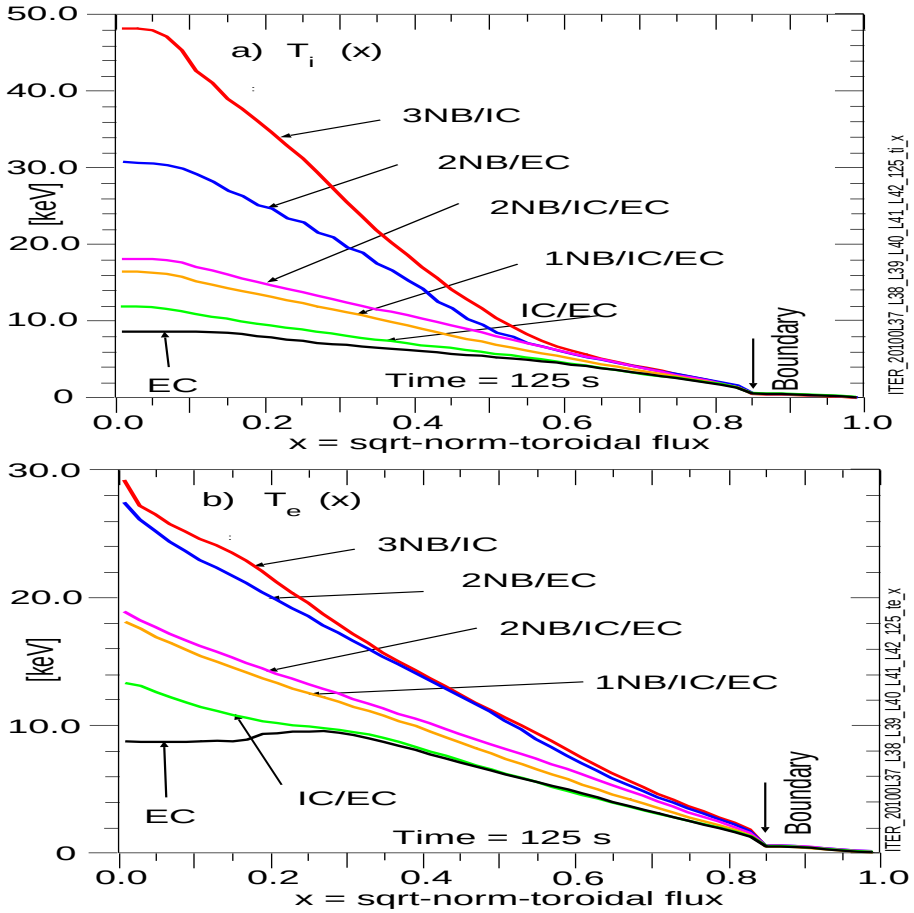

FIG. 10: (Color) a) Ion, and b) electron temperature profiles near the time when they are largest.

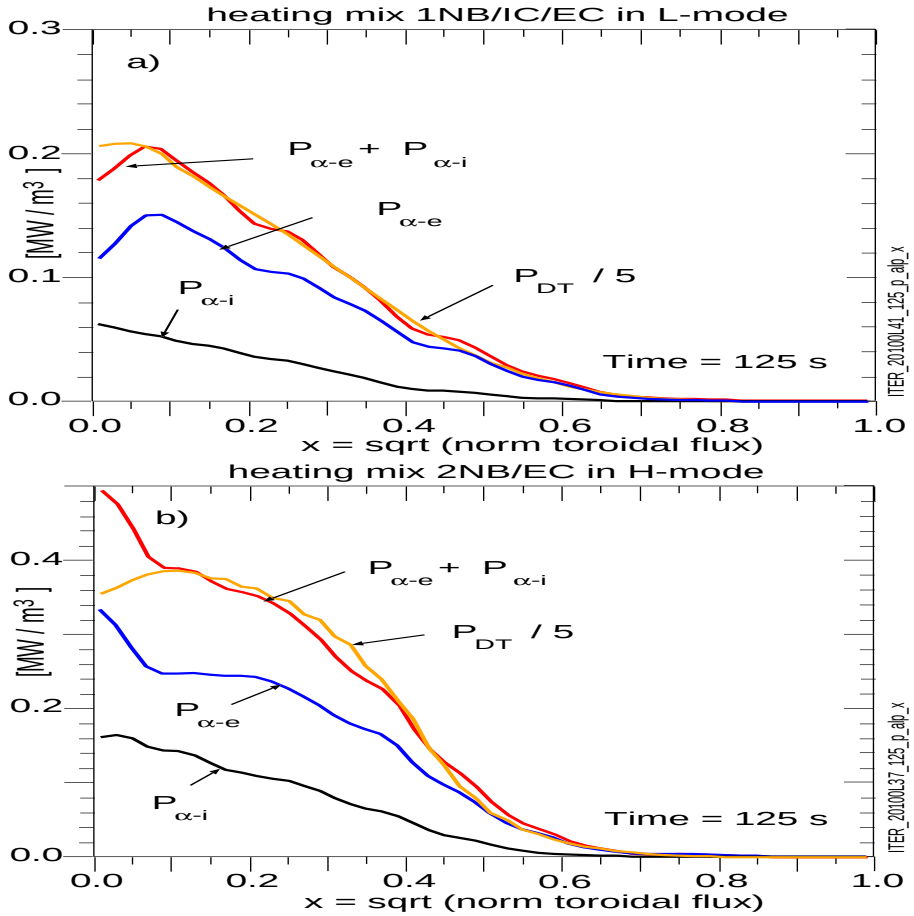

FIG. 11: (Color) Profiles of alpha powers to thermal electrons and ions and their total compared to the profile of $P_{\rm DT}$ / 5 assuming Option 2 when the $L \rightarrow H$ power threshold is assumed to be scaled up by a factor of 2. a) Heating mix that does not achieve H-mode; b) Heating mix that does achieve H-mode. The $\rm P_{\alpha-e}$+$\rm P_{\alpha-i}$ profile is close to the DT fusion power divided by five except for a dwell in time of approximately two sec due to the slowing down of the alpha particles. If a non-classical radial shift of fast alphas occurs (due, say to MHD or TAE activity) then the the shapes of the $P_{\rm DT}$ and alpha density profiles would differ.

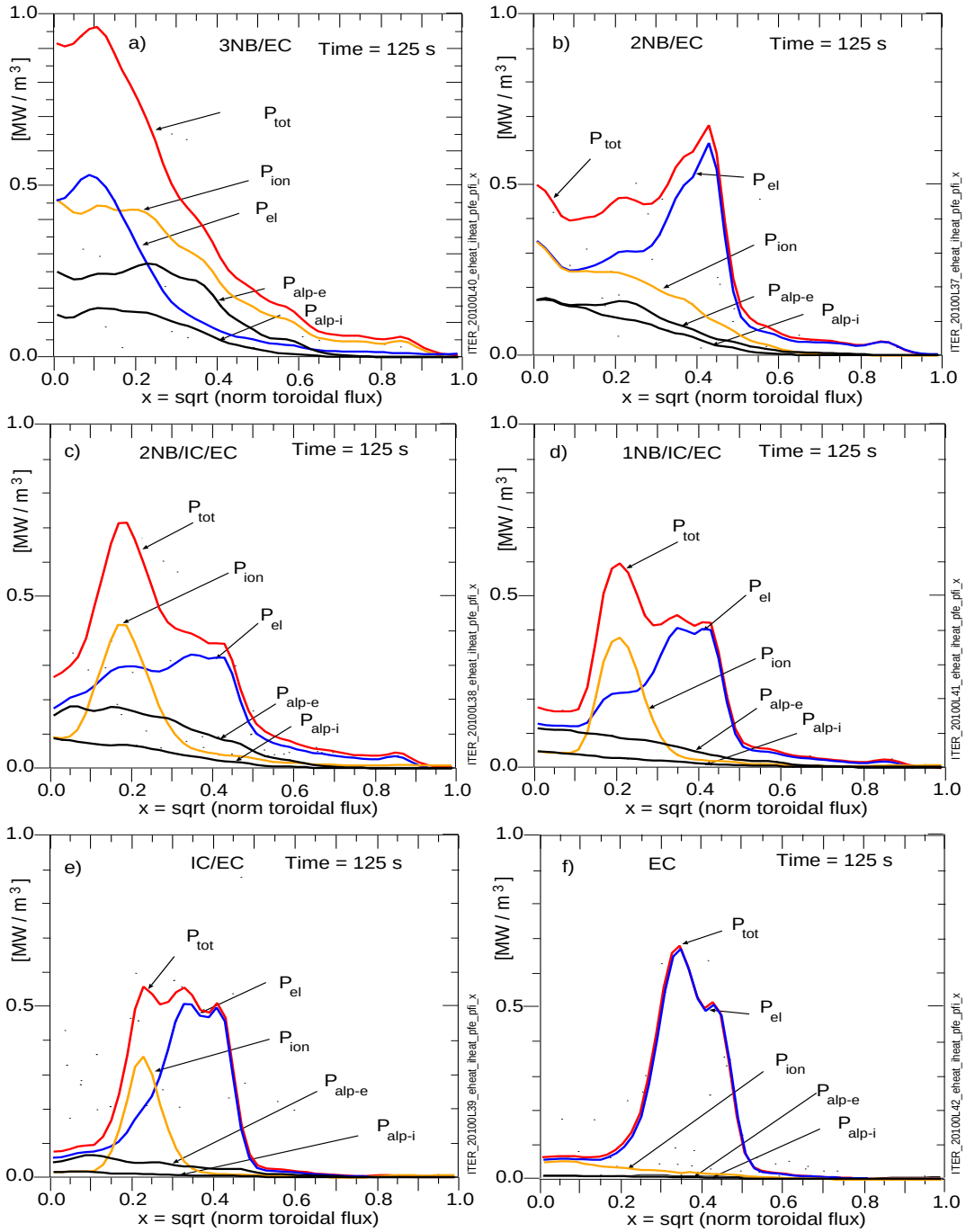

FIG. 12: (Color) Predictions of electron and ion heating using Option 2 late in the L-mode phase, two sec before the transition to H-mode. The alpha heating profiles are summed in the total ion and electron heating profiles.

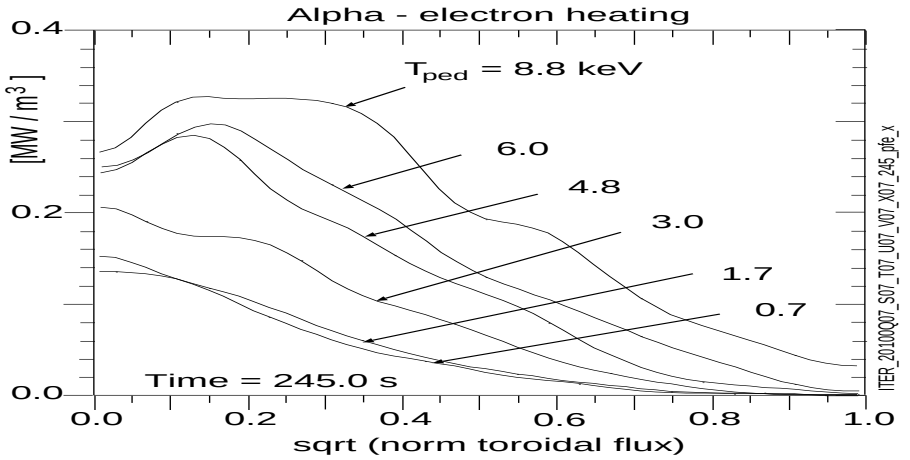

FIG. 13: Profiles of $P_{\alpha-e}$ at the flattop with $P_{\rm ext}$ = 73 MW.

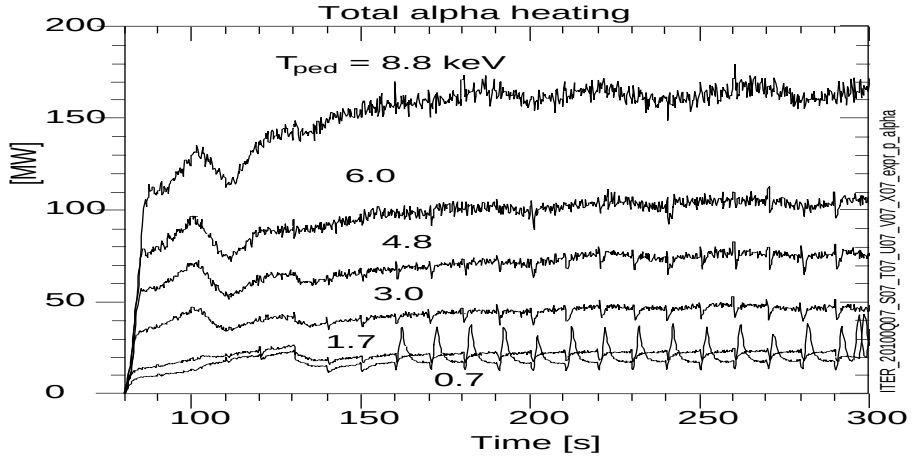

FIG. 14: Evolution of the total alpha heating for different assumptions for the pedestal temperature.

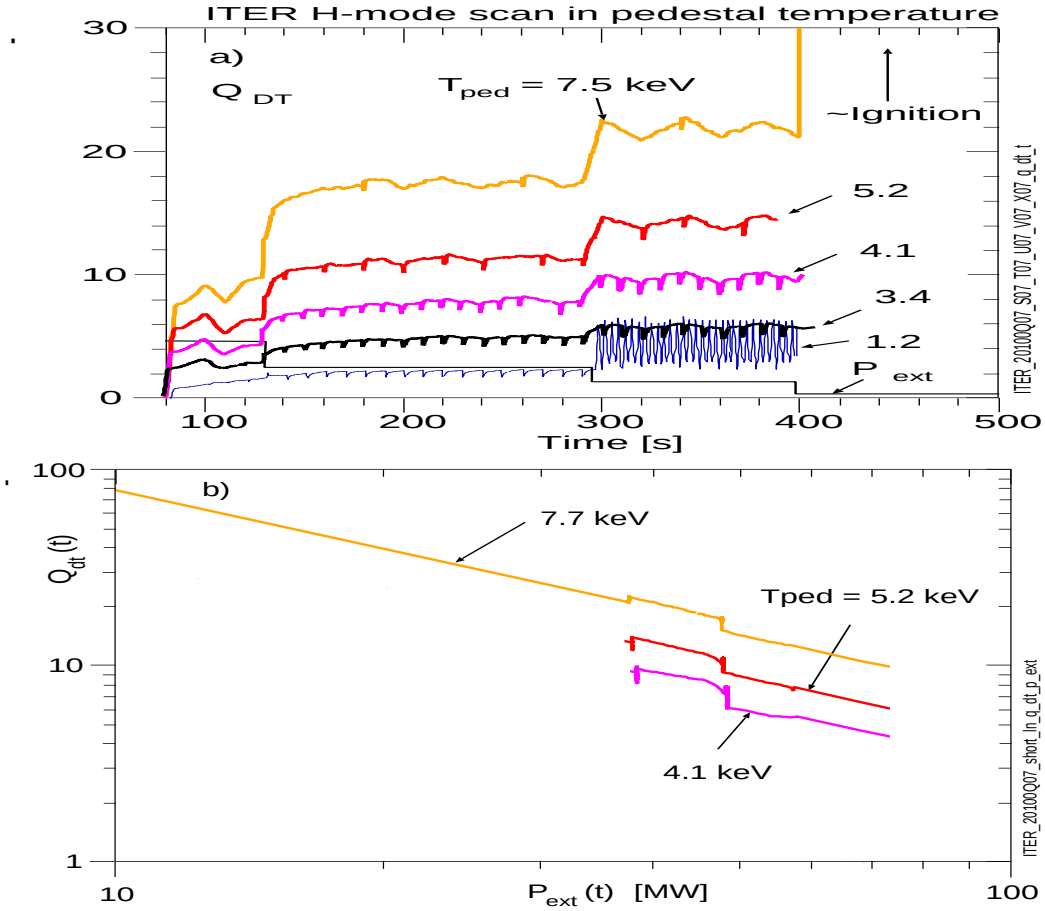

FIG. 15: (Color) a) Evolution of Q_{DT} for different assumptions for the pedestal temperature; b) scaling of $Q_{\rm DT}$ with $P_{\rm ext}$.

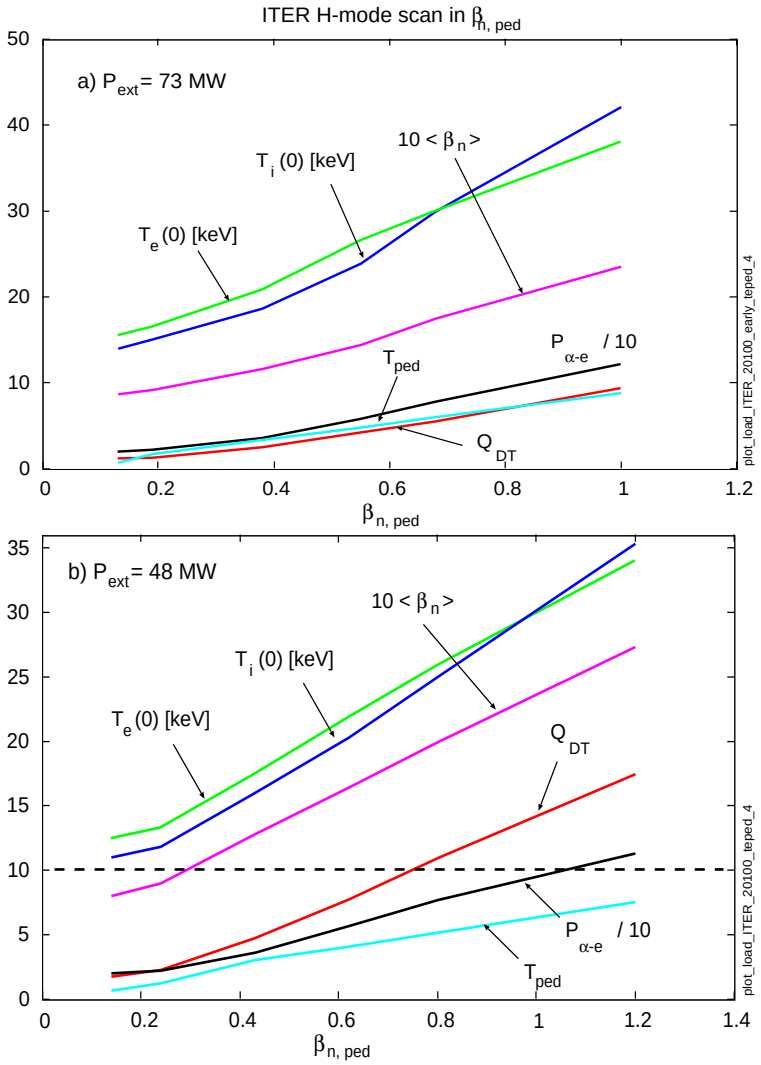

FIG. 16: (Color) Results with $P_{\rm ext}$ of a) 73 MW (115-120 s); b) 47 MW (245 s). The values of $\beta_{n,ped}$ given by the PEDESTAL module in PTRANSP are 0.38 for $P_{\rm ext}$ = 73 MW (corresponding to $T_i(0)$ = 18.6 keV), and and 0.43 for $P_{\rm ext}$ = 48 MW (corresponding to $T_i(0)$ = 16.0 keV). T$_{ped}$ or equivalently $\beta_{n,ped}$ is scaled up or down for the scaling study.

The Princeton Plasma Physics Laboratory is operated
by Princeton University under contract
with the U.S. Department of Energy.

Information Services
Princeton Plasma Physics Laboratory
P.O. Box 451
Princeton, NJ 08543

Phone: 609-243-2245
Fax: 609-243-2751
e-mail: pppl_info@pppl.gov
Internet Address: http://www.pppl.gov